



Dermatological expert system implementing the ABCD rule of dermoscopy for skin disease identification

Saptarshi Chatterjee^{a,*}, Debangshu Dey^a, Sugata Munshi^a, Surajit Gorai^b

^a Electrical Engineering Department, Jadavpur University, Kolkata 700032, India
^b Department of Dermatology, Apollo Gleneagles Hospital, Kolkata 700054, India

ARTICLE INFO

Keywords:
 Benign
 Dermoscopic images
 Expert system
 Malignant
 Skin disease

ABSTRACT

Doctors and radiologists generally follow the standard *ABCD* rule of dermoscopy for differentiating the malignant and benign skin lesions. The estimation of the dermoscopic score by visual inspection only, may lead to the inaccurate diagnosis of the disease at an early stage. In this work, the *ABCD* attributes have been improvised and quantified in a dermatological expert system (DermESy) for the differentiation of malignant and benign lesions. DermESy, a rule based expert system has been developed by implementing dermatologist's knowledge with proper quantification of the dermoscopic findings. Using DermESy, the dermoscopic images have been categorized as malignant, benign and suspicious lesions based on the estimated total dermoscopic score (*TDS*), similar to the findings of an expert. To estimate the *TDS*, shape, brightness and color variations are considered to modify the '*A*' score. The color information extraction algorithm is introduced to extract significant color regions to quantify the '*C*' score. To find the appropriate '*D*' score of a skin lesion, dermoscopic structures segmentation algorithms have been introduced. In this work, the *ABCD* rule of dermoscopy has been improvised by considering the spatial properties of dermoscopic structures for improved identification of malignant lesions. An explanatory subsystem is implemented in DermESy to assist the dermatologist with proper in-detail visualization. DermESy has differentiated the benign and malignant skin lesions with 97.69% sensitivity, 97.97% specificity and 97.86% accuracy. The *TDS* evaluated by DermESy is verified and compared against expert dermatologist's *TDS* scores of same dermoscopy images to establish the reliability and robustness of the proposed system.

1. Introduction

The early and accurate diagnosis of melanoma is important for further treatment and prevention of the disease. The complex structure, multiplicity of color and similarity in visual appearance make it difficult to differentiate malignant melanocytic lesions from other skin abnormalities (Marks, 1995). Dermatologists use epiluminescence microscopy or dermoscopy, a non-invasive and non-contact imaging technique, for the in-depth visualization of the pigmented area. The introduction of dermoscopy with detailed visualization of the skin lesion has increased the diagnostic accuracy by 5–30% (Pehamberger et al., 1993). Incorporating this screening tool, the dermatologists use clinical algorithms such as *ABCD* rule (Nachbar et al., 1994), and seven-point checklist (Argenziano et al., 1998; Kawahara et al., 2019) for the diagnosis of the skin diseases. The computer aided diagnostic system has come up with great possibilities in accurate diagnosis with quantification of the dermoscopic findings. The recent trends in the development of computer

aided diagnosis of skin diseases have assisted the clinicians and experts in investigating an outsized number of patients with higher diagnostic accuracy.

The *ABCD* rule of dermoscopy has been developed to quantify the dermoscopic findings for the diagnosis of the lesion under investigation. The *ABCD* rule of dermoscopy has incorporated the clinical criterion of the skin lesions such as asymmetry, border irregularity, color and differential structures. Combining these dermoscopic criteria, the total dermoscopic score (*TDS*) has been evaluated for the grading of the lesions as benign, suspicious or malignant. Computer aided diagnostic system has quantified the *ABCD* criterion and improved the diagnostic performance not only for the experts but also for clinicians with limited experience in dermoscopy. Kasmi & Mokrani (2016) have implemented the *ABCD* rule for the classification of malignant melanoma and benign skin lesions. For the estimation of the *TDS*, authors have used the shape, brightness and color asymmetry along with structural features for the improvement of the classification performance. Literature suggests

* Corresponding author.

E-mail address: saptarshichatterjee2009@gmail.com (S. Chatterjee).



different methodical approaches for the automatic diagnosis of skin lesions implementing the hand-crafted features (Ma & Tavares, 2017; Chandaka et al., 2009; Oliveira et al., 2016; Wahba et al., 2018; Chatterjee et al., 2018). The recent development in deep learning techniques have been used for skin disease identification by computer vision with impressive performance (Harangi, 2018; Yuan & Lo, 2019; Kawahara & Hamarneh, 2019; Gu et al., 2019). González-Díaz (2019) has introduced a convolutional neural network based approach, incorporating the knowledge of dermatologists for the identification of the skin lesions. The proposed system has lesion segmentation and dermoscopic structure segmentation blocks and has identified melanoma and seborrheic keratosis (SK) diseases with area under the curve of 87.3 and 96.2 respectively.

In this paper, a dermatological expert system (DermESy) for skin disease identification has been propounded. The reported expert system tool aims at assisting clinician and experts to provide a uniform, accurate and quick diagnosis along with monitoring of the skin lesions. To develop an indigenous integrated system with convenient visual monitoring of the dermoscopic findings, the following computing aids have been introduced in this work:

- Simple and efficient algorithms have been implemented to score the ABCD attributes.
- The estimation of total dermoscopic score (TDS) is reframed by improvised ABCD attributes. In addition to asymmetry in shape, brightness and color variations are also incorporated to reform the ‘A’ score.
- For ‘C’ score determination, a novel color information extraction module incorporating expert’s knowledge has been introduced to detect the significant dermoscopic colors. For the identification of significant color regions, the colors of the corresponding expert’s annotated regions from the same dataset are considered as reference.
- For pigment network and structureless area detection, mathematical morphology aided filtering technique is introduced. The irregular or localized distribution of the structure in the lesion area is more indicative towards melanoma than globally distributed structures. Considering this dermoscopic criterion, the ‘D’ score has been evaluated by not only considering the presence of the differential structures but also their spatially localized information.
- An explanatory subsystem is introduced to give the interpretations of the TDS so as to enable the analysis of the dermoscopic findings, and thus assist the expert to cross-verify the diagnosis by the DermESy.
- All the histopathologically confirmed dermoscopic images have been given to the dermatologist to segregate the malignant, benign and suspicious lesions. Dermatologist’s opinion has been compared with the performance of the DermESy for the differentiation of malignant and benign lesions. The dermoscopic findings as extracted from DermESy are correlated with the dermatologist’s assessment and a considerable improvement in diagnosis is successfully achieved, which satisfies the primary objective of this work.

The paper has been organized in the following manner. In Section 2, the implementation of knowledge-base module has been described, followed by dermatological informatics and rule base modules of the expert system in Section 3 and 4 respectively. In Section 5, the results have been discussed followed by the conclusion in Section 6.

2. Knowledge base for skin disease diagnosis

Expert system is an integrated computer aided decision-making system where expert’s knowledge, experience and skills are implemented using a rule-base for making proper inferences. A diagnostic expert system emulates the expertise of an experienced doctor, having specific domain knowledge, essentially by the following major components.

- Knowledge Base and Rule base
- Inference Engine
- User Interface

The block diagram of a diagnostic expert system has been shown in Fig. 1. The knowledge base of the DermESy contains the experts’ understanding based on clinical ‘naked eye’ observation of the skin abnormalities. It has replicated the dermatologist’s knowledge to formulate the ABCD rule for the characterization of skin lesions.

2.1. ABCD rule of dermoscopy

The ABCD algorithm has been developed to quantitatively address the crucial dermoscopic criteria such as asymmetry (A), border (B), color (C) and differential structures (D).

- Asymmetry: The structural variation along the entire lesion is considered to differentiate the benign and the malignant lesions clinically. The criterion encompasses both contour asymmetry and the disproportionate distribution of dermoscopic color, luminance and structures along the lesion area.
- Border: To assess whether there is an abrupt cutoff of pigment pattern at the periphery of the lesion, or a gradual indistinct cutoff, the border irregularity has been estimated.
- Color: The presence of one or more colors or an uneven distribution of color is taken into account by the dermatologist for the early stage diagnosis of the lesion.
- Differential structures: For the characterization of skin lesion, presence of differential structures is considered to be an important dermoscopic finding. To determine the dermoscopic structural features, presence of structureless area, pigment network, branched streaks, blue-white veil, dots and globules have been given the major consideration. To estimate the dermoscopic score for differential structures, a maximum of five score is allotted, one score to each structure.

3. Dermatological informatics module implementing ABCD rule

The dermatological informatics module (DIM) contains the significant information regarding the skin lesion characteristics. This block is dedicated to extract the essential dermoscopic findings for logical construction of rule base.

DIM extracts the significant information regarding the skin lesion characteristics. This block is dedicated to extract the essential

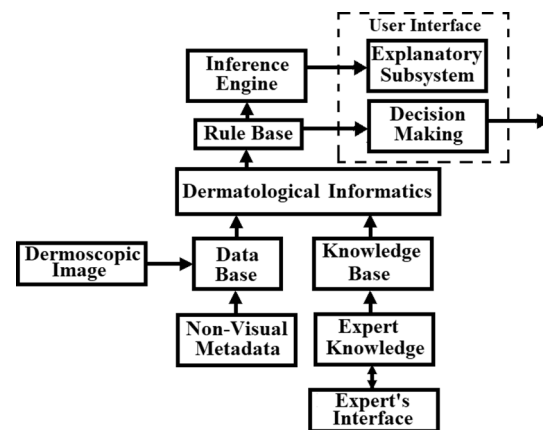


Fig. 1. Block diagram of the Dermatological Expert System.

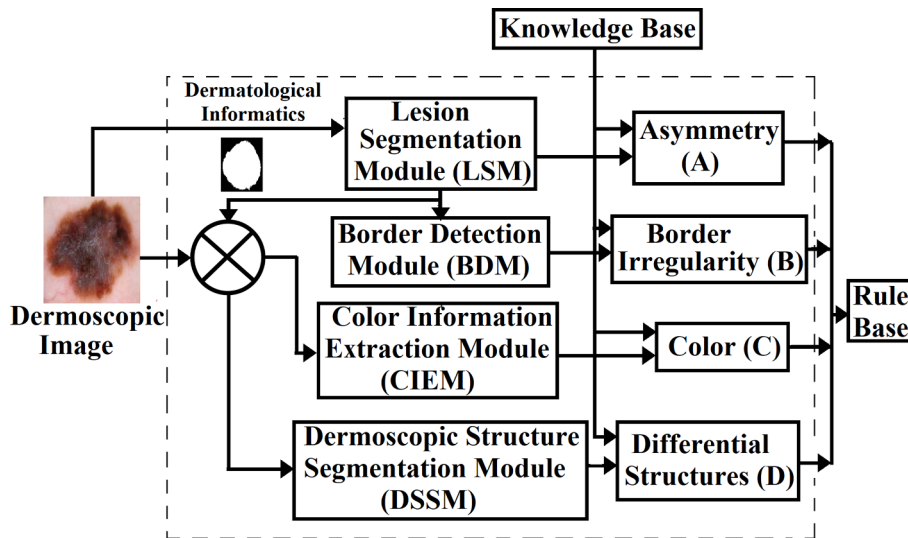


Fig. 2. Detailed block diagram of Dermatological Informatics module.

dermoscopic findings for logical construction of rule base. The main pipeline of the dermoscopic ABCD clinical feature extraction is depicted in Fig. 2. For each clinical case, the dermoscopic image (I) has been preprocessed for the removal of noise and hair artifacts. The pre-processed image is considered by the lesion segmentation module (LSM) to segregate the region of interest (ROI). From the segmented image, shape asymmetry of the lesion has been evaluated to compute the asymmetry index ('A' attribute of ABCD rule). The segmented image has been fed to the border detection module (BDM) for outlining the single pixel border of the lesion area. The border detected image is used to estimate the border irregularity ('B' attribute of ABCD rule) of the lesion area. Original color dermoscopic image has been masked with the segmented image to separate out the clinically significant dermoscopic color regions from the lesion area using the color information extraction module (CIEM). CIEM subsystem helps to determine the color asymmetry of the lesion ('A' attribute of ABCD rule) and also to find the dermoscopic colors present in the lesion ('C' attribute of ABCD rule). Segmented image masked with the original gray scale image is used to estimate the brightness asymmetry ('A' attribute of ABCD rule) present in the lesion area. The same gray scale image has been used as an input to the dermoscopic structures segmentation module (DSSM) to extract differential structures from the skin lesion. The dermoscopic structures segmented using DSSM subsystem has been used to compute the 'D' score of the ABCD rule. For the estimation of the 'D' score, spatial information of the differential structures has been considered to develop an improvised ABCD rule of dermoscopy.

Description of all the modules considered for the excavation of ABCD dermoscopic features have been given in detail in the subsequent sections.

3.1. Image pre-processing

In the preprocessing stage, a median filter is used to eliminate the noise due to uneven illumination. Dermoscopic images of skin lesions from various anatomic sites are contaminated with thick or thin hairs. To remove these hair artifacts, the morphological bottom-hat filter (Soille, 2004) with varying size of the structuring element followed by the inward interpolation technique has been implemented (Chatterjee et al., 2019a,b). Presence of hair structures through the lesion border region extends the lesion area and introduces unwanted over-

segmentation of the region. Elimination of hair artefacts helps to obtain appropriate segmented region for further analysis and estimation of dermatological properties of the lesion.

3.2. Lesion segmentation module

After preprocessing, segmentation of lesion area is an essential step for skin disease identification and monitoring of further spreading of the disease. In DIM, the *lesion segmentation module* is implemented to segregate the affected area from the dermoscopic image. Dermatologists mark the lesion area manually to estimate the amount of pigmentation compared to that in the normal skin area. Proper segmentation of the lesion helps to determine the morphological properties of the pigmented area and to evaluate the asymmetry index of the region of interest. Mathematical morphology aided skin lesion segmentation algorithm has been developed in the LSM sub-system. The fundamental element of mathematical morphology is the structuring element (SE) (Soille, 2004). Selection of appropriate SE is important for the development of algorithms using morphological operations. The shape of the structuring element should be selected according to the morphological properties of the object under consideration. In this work, most of the skin lesions are circular in nature or closer approximation of a circle. Therefore, to segmentize the skin lesions using morphological operations, circular structuring element or a circular kernel comparatively smaller in size has been considered. For the development of morphological filters and segmentation algorithm, same form of circular SE has been considered for all the dermoscopic images of the entire dataset. For the development of mathematical morphology aided segmentation algorithm, the size of the circular structuring element has been chosen with a size of eight-pixel diameter. Gray scale morphological closing operation has been performed on the original gray scale image to remove smaller objects compared to the size of the SE. Subtracting the complement of the image from the closed image results a sharp contrast between the lesion and surrounding background. The maximum inter-class variance of the image is measured to estimate a threshold value for the segregation of the region of interest (Chatterjee et al., 2019b). In Fig. 3, segmented regions of sample dermoscopic images of malignant and benign category have been shown. From the figure, it has been observed that even having significant variations in morphological properties, the reported segmentation algorithm has effectively segmented the

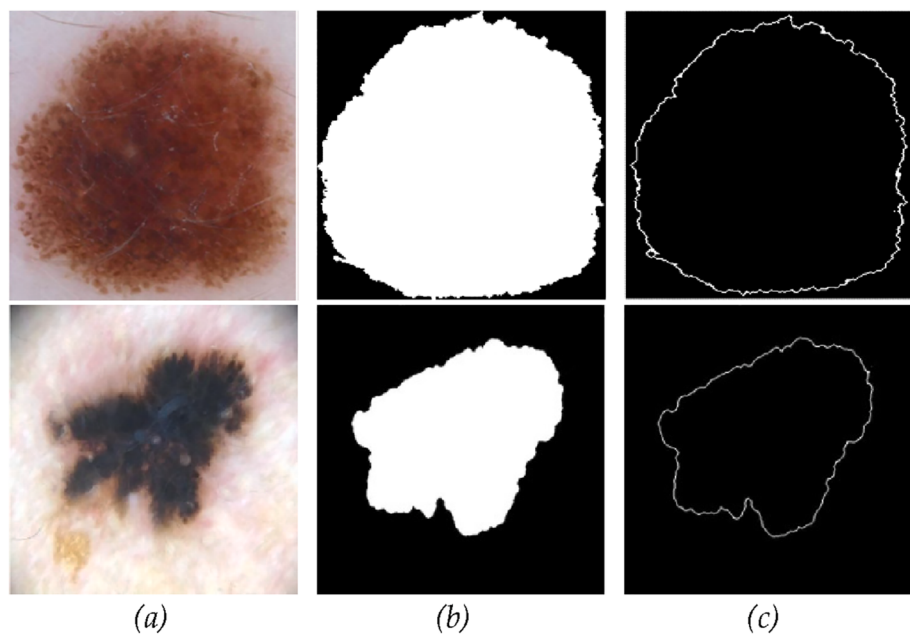


Fig. 3. (a) Original dermoscopic image, (b) Segmented image and (c) Border image.

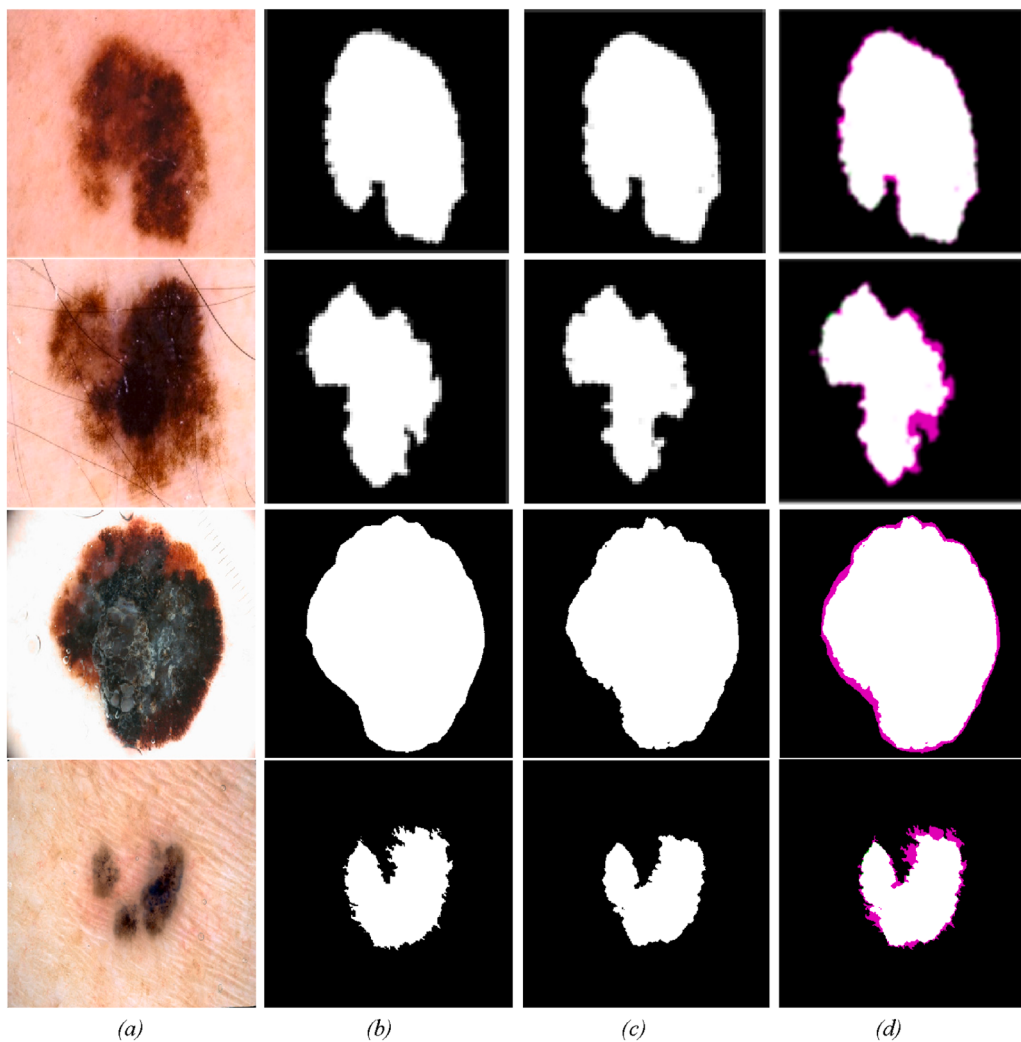


Fig. 4. (a) Original images, (b) Segmented ground truth images, (c) Segmented images using LSM, (d) Similarity measure of the segmented image with respect to the ground truth image.

appropriate region of interest.

3.2.1. Performance evaluation of LSM subsystem

The performance of the LSM sub-system has been determined by the quantitative estimation of the similarity between the segmented lesion and its corresponding ground truth (GT) image. The ground truth images have been annotated by an expert dermatologist. The similarity measure between the segmented images and corresponding GTs of the sample dermoscopic images have been shown in Fig. 4. In Fig. 4, images in the second column correspond to the GT images while the third column represents the segmented images obtained using LSM subsystem. In Fig. 4(d) the pink color has indicated the amount of dissimilarity between the segmented image and the corresponding GT. From the resultant image, it has been observed that the reported morphological segmentation algorithm has segregated the region of interest with much closer approximation to the GT images. The lesions with complex structure and various shapes have been segmented using the morphology aided segmentation technique with circular structuring element. The selection of circular structuring element has also improved the segmentation performance and makes the algorithm robust.

The goodness of segmentation has been evaluated by estimating the pixel level sensitivity (*Sen*), specificity (*Spc*) and accuracy (*Acc*) (Chatterjee et al., 2019; Pal et al., 2019) along with the similarity measure indices as Jaccard similarity index (*JSI*) and dice similarity coefficient (*DSC*) (Chatterjee et al., 2019; Pal et al., 2019). The segmentation performance indices have been defined as the following.

$$\text{Sensitivity } (\text{Sen}) = \frac{TP}{TP + FN} \quad (1)$$

$$\text{Specificity } (\text{Spc}) = \frac{TN}{TN + FP} \quad (2)$$

$$\text{Accuracy } (\text{Acc}) = \frac{(TP + TN)}{(TP + TN + FP + FN)} \quad (3)$$

Here, *TP*, *TN*, *FP* and *FN* denote the number of true positive, true negative, false positive and false negative pixels respectively (Chatterjee et al., 2019; Pal et al., 2019). Therefore, the standard notations *TP*, *TN*, *FP* and *FN* for segmentation performance evaluation have been defined as,

TP = pixels correctly segmented as foreground or ROI; *TN* = pixels correctly detected as background; *FP* = pixels wrongly detected as foreground or ROI; *FN* = pixels wrongly detected as background.

Considering, the segmented image (*I*) and its corresponding ground truth image (*G*) as two sets, *JSI* and *DSC* can be expressed as the following.

The Jaccard similarity index of two sets (Chatterjee et al., 2019; Pal et al., 2019) is expressed as:

$$\text{JSI}(I, G) = |I \cap G| / |I \cup G| \quad (4)$$

Where, $|I|$ represents the cardinality of set *I*. The *JSI* can be expressed in terms of *TP*, *FP* and *FN* as (Chatterjee et al., 2019; Pal et al., 2019):

$$\text{JSI}(I, G) = \frac{TP}{TP + FP + FN}. \quad (5)$$

Similarly, the dice similarity coefficient of two sets *I* and *G* is expressed as (Chatterjee et al., 2019; Pal et al., 2019):

$$\text{DSC} = 2 \times |I \cap G| / (|I| + |G|). \quad (6)$$

Where, $|I|$ represents the cardinality of set *I* and $|G|$ represents the cardinality of set *G*. The *DSC* could be expressed in terms of *TP*, *FP* and *FN* as the following (Chatterjee et al., 2019; Pal et al., 2019).

Table 1
Performance of The LSM Sub-System.

Data Base	Values	Segmentation Performance Indices				
		Sen	Spc	Acc	JSI	DSC
ISIC& PH2Dataset	Min	0.606	0.626	0.710	0.658	0.662
	Max	0.997	0.996	0.989	0.897	0.927
	Avg	0.917	0.974	0.962	0.834	0.884

$$\text{DSC}(I, G) = 2 \times \frac{TP}{(2 \times TP + FP + FN)}. \quad (7)$$

The segmentation performance indices of the entire dataset considered in this work has been tabulated in Table 1. The estimated performance indices from table 1 describe the goodness of the segmentation algorithm implemented in LSM subsystem for the segmentation of wide varieties of lesions. The table shows the minimum and maximum values of the performance indices obtained from the entire dataset. Minimum values of *JSI* and *DSC* correspond to the significant deviation of the segmented image and corresponding ground truth image. Similarly, the maximum values indicate closer similarity between the resultant image and its corresponding ground truth. However, the sufficiently large average values of performance indices have testified the closeness of the segmented image and its corresponding ground truth (GT) for maximum number of images in the dataset. Therefore, the acceptable segmentation performance indices ensure the accurate segmentation of small as well as complex structures of various skin lesions.

3.3. Border detection module

The segmented image (I_S) is considered in the subsequent border detection module to obtain a single pixel border of the lesion area. For the determination of single pixel border of the segmented region, two-pixel diameter has been considered for the circular SE. Selection of larger SE thickens the border region of the segmented image and the proper estimation of the irregularity is not possible (Soille, 2004). Morphological erosion operation on the segmented image eliminates the abrupt changes along the border region (Soille, 2004). Morphological gradient operation, i.e. subtraction of the eroded image from the segmented image is performed to obtain the appropriate border of the lesion area. The structural variations obtained from the resultant border image is used to estimate its irregularity. The corresponding border regions of the segmented lesions have been shown in Fig. 3(d).

3.4. Color information extraction module

As explained in the previous section, dermatologist has explored the occurrence of six different colors (white, red, light brown, dark brown, blue-gray and black) for the diagnosis of the skin lesion. This color information has been extracted from a set of sample images, consulting with an expert dermatologist. A set of sample dermoscopic images of different classes are given to the experienced dermatologist to mark the above mentioned significant color regions. In Fig. 5, the ground truth images, identifying light brown, dark brown, red and black regions have been shown. The intensity values of each color plane of corresponding color have been considered as reference information for the development of the color information extraction algorithm.

The input dermoscopic image masked with the corresponding segmented image (I, I_S) has been considered to develop the color information extraction algorithm. To sub-divide the skin lesion area with similar color regions, superpixels are generated by applying simple linear iterative clustering (*SLIC*) algorithm (Achanta et al., 2010). Here, the desired size of the superpixel is chosen as the input parameter in contrast to the number of superpixels as considered in *SLIC* algorithm. For an image with total *P* pixels, the number of superpixels, each with *N* pixels, is P/N . The histogram (*hist*) of an image describes the frequency of occurrence of the intensity present in that image. Therefore, in histogram, the intensity value with maximum number of bins determines the dominant color information of each superpixel region. The distance (D_c) between the prevailing color (C_{RGB}) in a superpixel region and the corresponding reference has been estimated. If this measured distance is less than the just noticeable distance (Kasmi & Mokranim, 2016), the entire superpixel region will be replaced by the dominant color. In Algorithm1, the color information extraction technique has been described. For two dermoscopic sample images, their corresponding

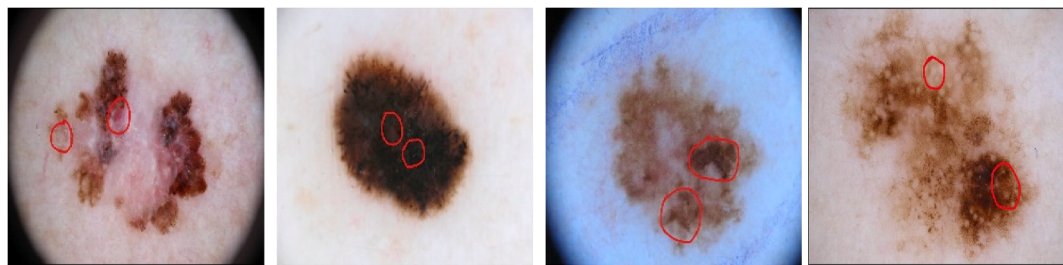


Fig. 5. Ground truth images with different color regions (light brown, dark brown, red, black) marked by the expert dermatologist.

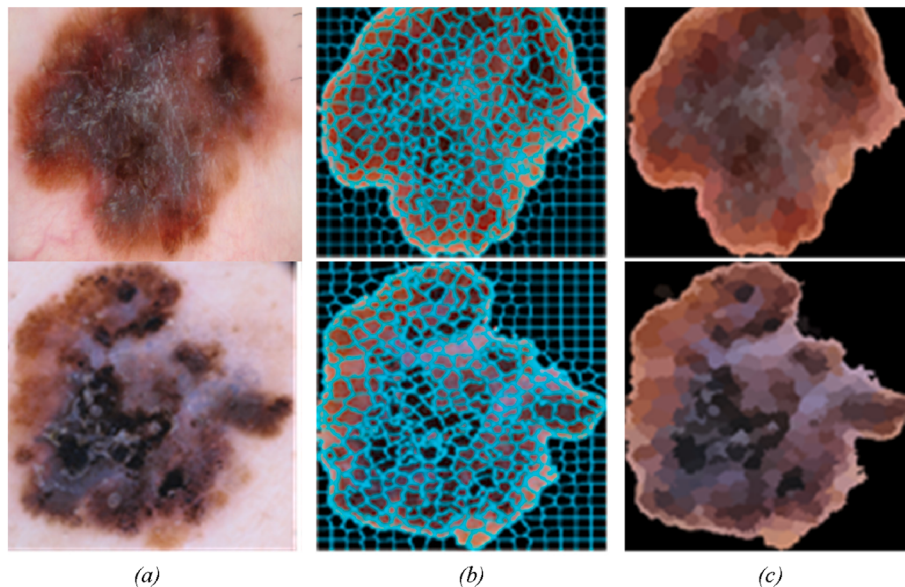


Fig. 6. (a) Original dermoscopic images, (b) Superpixel regions and (c) Identified color regions.

superpixel regions and extracted color regions have been shown in Fig. 6.

Algorithm1: Color information extraction

Input: Dermoscopic image I in RGB color plane; R, G, B values of six reference colors, W (white), R (red), LB (light brown), DB (dark brown), BG (blue-gray), B (black); segmented image I_s ; superpixels containing N number of pixels.

Output: I_c : Image with identified color regions

Step-1 Compute P , the number of pixels present in the segmented image I_s .

Step-2 Mask the input image I with the I_s to obtain the masked image I_m .

Step-3 Initialize the number of pixels N to form a superpixel.

Step-4 Determine the desired number of superpixels $S = P/N$.

Step-5 Consider I_m and S as input parameters for SLIC algorithm to obtain the labeled image I_L and number of superpixels S_o

Step-6 From each label L of the superpixel regions I_L , determine the maximum intensity value C_{RGB} as the intensity value having maximum number of bins in the image histogram ($hist(I_L)$). Determine the just noticeable distance D_c of the prevailing color C_{RGB} from the reference colors to obtain the image with identified color regions I_c as the following:

```

for L = 1 : S_o
    CRGB = max(hist(IL(L)))
    Dc = dist(CRGB, W, R, LB, DB, BG, B)
    If Dc < 6 do
        Ic(L) = CRGB
    end
end

```

Step-7 Obtain the image with identified color regions by repeating the Step-6 for each label L .

For the development of DermESy five dermoscopic structures considered here are pigment network, dots, globules, structureless area and blue-white veil. Presence of different differential structures helps to differentiate malignant and benign lesions. Different signal processing tools have been introduced to extract those five differential structures from the dermoscopic images. Consulting with expert dermatologist the algorithms have been modified to include expert's knowledge.

3.5.1. Pigment network detection

This is considered to be an important dermoscopic structure for identifying melanocytic skin lesions. This differential structure usually formed as a reticular pattern in a lighter

background, is distributed in regular or irregular mesh along the lesion (Barata et al., 2012; Pathan et al., 2018). For its detection, morphological bottom-hat filtering with linear SE has been applied on the dermoscopic image masked with the segmented image. Bottom-hat filter extracts the structures having intensity darker than their surroundings. The filtered image is passed through a bank of directional filters, to obtain the connected reticular patterns in different directions.

Since, the pigment network is distributed along the lesion with different orientations, $N + 1$ filters are developed. For the development of directional filter bank, the orientation θ_d has been considered as, $\theta_d \in [0, \pi]$, $d = 1, \dots, N$. Here, twelve directions ($d = 12$) are considered with an incremental steps of $\pi/15$. The impulse response is given by (Barata et al., 2012),

$$P_{\theta_d} = G_1(x, y) - G_2(x, y). \quad (8)$$

where, 2D Gaussian filter G_n is given as:

3.5. Dermoscopic structure segmentation module

The DSSM subsystem determines the dermoscopic findings that correspond to the local and global structures present in the lesion area.

$$G_n(x, y) = k \exp \left\{ -\frac{x'^2}{2\sigma_{xn}^2} - \frac{y'^2}{2\sigma_{yn}^2} \right\}, \quad n = 1, 2. \quad (9)$$

Here, k is the normalization constant and the values of (x', y') are related to (x, y) as,

$$x' = x \cos \theta_d + y \sin \theta_d. \quad (10)$$

$$y' = y \cos \theta_d - x \sin \theta_d. \quad (11)$$

The image is filtered by each directional filter and maximum operation is performed at each pixel (x, y) of the output image to obtain the pigment network as a grid of thin lines. In Fig. 7, the segmented pigment networks and corresponding regions in the lesion area are shown for two sample dermoscopic images.

3.5.1.1. Performance evaluation of pigment network detection system. Performance of the reported pigment network detection system has been evaluated by considering the relevant ground truth images provided in the ISIC archive database. The corresponding pigment network regions of a skin lesion area are marked in the ground truth images by the dermatologists. Therefore, the similarity measure between the detected pigment network and corresponding GT describes the effectiveness of pigment network detection algorithm. Performance of the algorithm has been evaluated by estimating pixel level sensitivity (*Sen*), specificity (*Spc*), accuracy (*Acc*), similarity co-efficient of Jaccard index (*JSI*) and dice similarity coefficient (*DSC*) as given in Table 2. From the table, the minimum values of performance indices correspond to the variations of the detected region from the GT and the maximum values determines the maximum similarity between the detected region and corresponding ground truth. Considering the lesions containing pigment network, the average values of the performance indices have been determined. The acceptable values of the performance indices demonstrate the identification of pigment network for maximum number of images with higher degree of similarity with the GTs.

Algorithm 2: Dots and Globules Detection

Input: Original gray scale image I_g ; segmented image I_s ; threshold sensitivity (T_s); minimum radius $R_{min}R_n$ of the circular structuring element SE in pixels; maximum radius R_{max} of the circular structuring element SE in pixels.
Output: I_o : Dots & Globules detected image.
Step-1 Mask the input image I_g with I_s to obtain the masked image I_m .
Step-2 Initialize the input variables as $T_s = 0.02$; $R_{min} = 2$; $R_{max} = 8$.
Step-3 Obtain the resultant image I_o with segmented dots and globules by employing varying size of the SE from R_{min} to R_{max} as:
3.1 for each radius r from R_{min} to R_{max} with an increment of 2 pixels do:
3.2 form the circular SE for each radius r .
3.3 obtain the closed image I_c by applying morphological closing operation on I_m using circular SE .
3.4 apply morphological reconstruction of I_c under I_m by considering 4-connected neighboring pixels to obtain the reconstructed image I_R .
3.5 apply the morphological bottom-hat filter by subtracting I_g from I_R to obtain the image I_d with the extracted objects having smaller in size compared to r and intensity darker than their surroundings.
3.6 estimate the minimum intensity I_{dmin} present in the extracted regions in I_d .
3.7 estimate the maximum intensity I_{dmax} present in the extracted regions in I_d .
3.8 calculate the threshold value $T_h = T_s \times (I_{dmax} - I_{dmin}) + I_{dmin}$.
3.9 segment the objects in I_d having intensity greater than T_h to obtain the dots and globules detected image I_o .
3.10 repeat step 3.1 to 3.9.
Step-4 Aggregate all the resultant images I_o to extract dots and globules from the input image.

3.5.2. Dots and globules detection

Circular or oval shaped dots and globules of various sizes are present throughout the lesion. The dots are smaller in size while the globules occupy some considerable area. To extract the dot/globule like structures, morphological bottom-hat filter has been employed with circular structuring element of varying size. The diameter of the SE has been

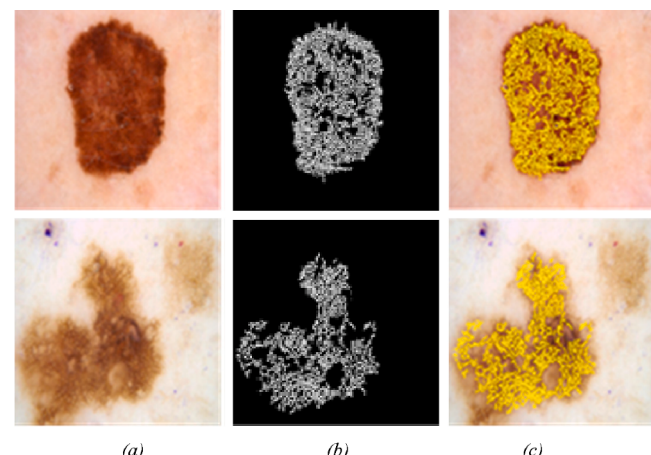


Fig. 7. (a) Original dermoscopic images, (b) Segmented pigment network and (c) Detected pigment network overlaid on the original image.

varied from minimum value of two-pixels to maximum radius of six pixels. For the segmentation of the dots and globules, the threshold value has been determined by estimating the difference of minimum and maximum intensities of the corresponding regions, as given in Algorithm2. Dots and globules detected regions from sample dermoscopic images have been shown in Fig. 8.

From Fig. 8, it has been observed that morphological filter with varying size of structuring elements have extracted dots and globules of different sizes. The figure describes that the globules have been found in the malignant lesion, which helps to differentiate it from benign lesions.

3.5.2.1. Performance evaluation of dots and globules detection system. To evaluate the performance of the morphological filter aided dots and globules detection algorithm, corresponding GT images given in ISIC archive dataset have been considered. As tabulated in Table 3, pixel level sensitivity (*Sen*), specificity (*Spc*), accuracy (*Acc*) are determined and the degree of similarity between the segmented dots, globules regions and corresponding GT are determined by *JSI* and *DSC*. Table 3 shows the minimum, maximum and average values of performance indices for dots and globules detection. The acceptable values of *JSI* and *DSC* describe the detection of dots and globules with high degree of similarity.

3.5.3. Detection of structureless area of skin lesion

Few areas in dermoscopic images are devoid of any pigment network or any other structures like globules, flat or elevated areas. These are called structureless area. Their size is regarded to be at least 10% of the total lesion area. Structureless area can be hypo, hyper or with regular pigmentation. In dermoscopic images, the structureless area has closely similar intensity variation as normal skin region. To extract the structureless area from the lesion, mathematical morphology aided technique is employed. The segmented image of the corresponding original dermoscopic image has been considered as mask to identify the lesion area from the original image. The morphological closing operation has been performed using circular structuring element of 4-pixel diameter on the gray scale lesion image masked with the original image. The closing

Table 2

Performance Evaluation of Pigment Network Detection System of The DSSM Sub-System.

Structures	Values	Segmentation Performance Indices				
		<i>Sen</i>	<i>Spc</i>	<i>Acc</i>	<i>JSI</i>	<i>DSC</i>
Pigment Network	Min	0.562	0.545	0.556	0.591	0.572
	Max	0.953	0.961	0.963	0.876	0.869
	Avg	0.914	0.925	0.913	0.806	0.811

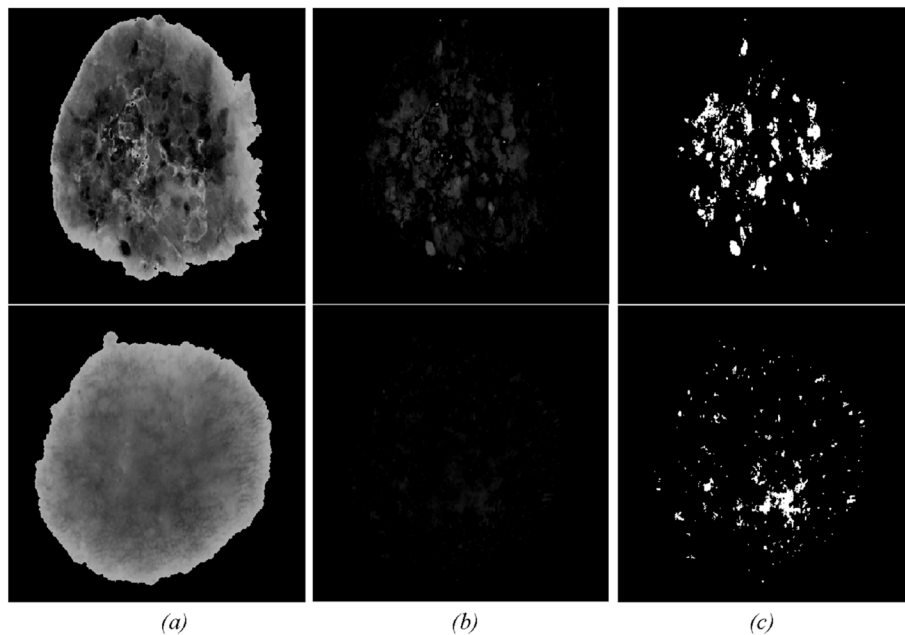


Fig. 8. (a) Original dermoscopic images masked with the corresponding segmented image (b) Extracted dots and globule regions (c) Detected dots and globules.

Table 3
Performance Evaluation of Dots and Globules Detection System of The DSM Sub-System.

Structures	Values	Segmentation Performance Indices				
		Sen	Spc	Acc	JSI	DSC
Dots & Globules	Min	0.581	0.569	0.603	0.537	0.541
	Max	0.981	0.977	0.983	0.881	0.863
	Avg	0.913	0.935	0.930	0.865	0.871

operation eliminates the small objects compared to the size of the structuring element. Subtraction of the complement of the original image from the closed image provides a significant intensity variation between the structureless uniform region and the pigmented region of the skin lesion. From the resultant image, the threshold value has been determined by selecting the maximum intra class variance of the lesion area with subsequent extraction of the structureless area. [Fig. 9](#) depicts the original dermoscopic image and corresponding structureless area.

[Fig. 9\(c\)](#) exhibits the distinguished intensity variations present in the structureless area and pigmented region after applying the morphological gradient operation. The extracted structureless areas have been portrayed in [Fig. 9\(d\)](#).

3.5.4. Detection of Blue-white veil of skin lesion

Blue-white veil is a focal bluish structure with an overlaying ground glass appearance. It is mainly a raised or clinically palpable component. Histologically, it represents highly pigmented melanocytes or melanoophages or melanin within the dermis. Blue-white veil is usually found in melanoma but may also be present in Spitz nevus. To extract the blue-white veil from the lesion, the input color dermoscopic image has been masked with the corresponding segmented image to confine the findings within the lesion area only. For the identification of blue-white veil, the simple linear iterative clustering (SLIC) algorithm has been considered. SLIC algorithm subdivides the region of interest into smaller superpixels depending on the present color information. From each of the superpixel region, mean intensity values of each R, G and B plane have been

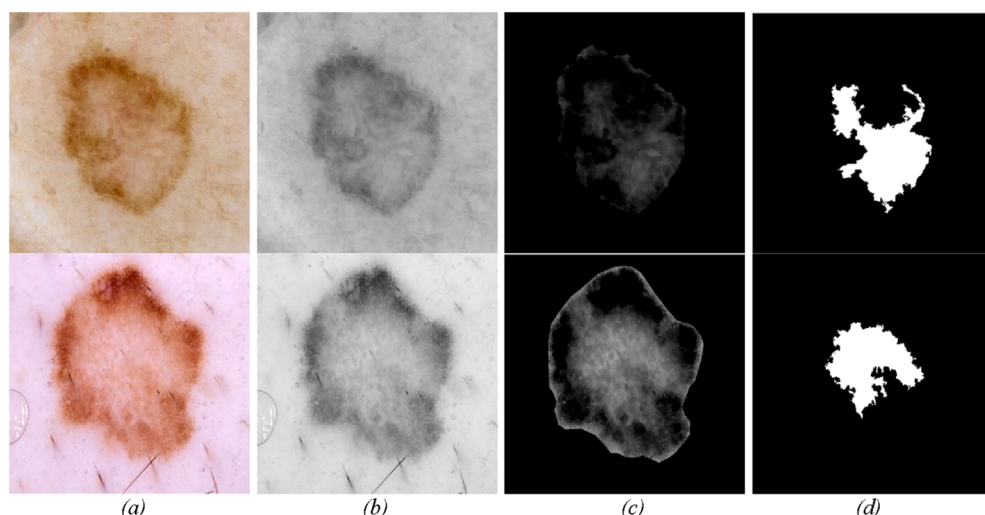


Fig. 9. (a) Original dermoscopic images; (b) Gray scale image; (c) Original masked with the corresponding segmented image after morphological gradient operation; (d) Extracted structureless area.

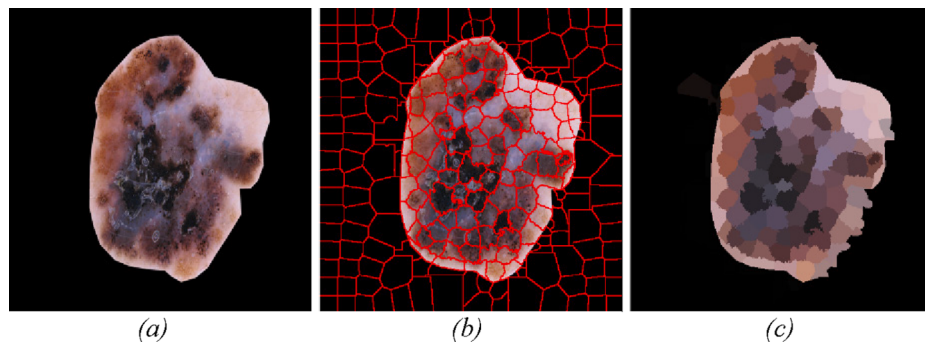


Fig. 10. (a) Original dermoscopic images masked with the corresponding segmented image; (b) Superpixel regions; (c) Identified blue-white veil regions.

estimated. Measuring the distance between the mean intensity of each superpixel region and corresponding reference values as annotated by the dermatologist, the blue-white veil regions have been identified. Fig. 10 depicts the original dermoscopic images and its corresponding superpixel regions. In Fig. 10(d) blue-white veil regions have been observed according to their mean values.

4. Rule base design

The rule-base module has been incorporated for obtaining the total dermoscopic score (*TDS*) and finally, for the detection of the disease. It has been designed for the parameter estimation of asymmetry (*A*), border irregularity (*B*), color (*C*) and differential structures (*D*). For an input dermoscopic image, the estimated values of the *ABCD* attributes will act as correlated information for the explanatory subsystem module. Similarly, the estimated *TDS* has been used for the design of rule-based disease classification technique as an integrated part of decision making module.

4.1. Rule base design to determine the total dermoscopic score

4.1.1. Asymmetry

The asymmetry estimation considers shape, brightness and the color asymmetry with respect to the horizontal and vertical axes, crossing the center of gravity of the segmented lesion. To estimate the asymmetry of the lesion, an asymmetricity score has been assigned from the minimum value of 0 to the maximum value of 2. If asymmetry (considering shape, brightness and color) is absent with respect to both the axes then the asymmetry score is zero. For single axis asymmetry, the asymmetricity score has been scaled as 0.25 for the asymmetry with respect to any one parameter (shape, brightness and color), 0.5 for any two parameters and 1 for all the parameters. Similarly, for both axes asymmetry, the asymmetricity score has been scaled as 1.25, 1.5 and 2 for the asymmetry of single parameter, any two parameters and all parameters respectively.

To estimate the shape asymmetry, the difference between the areas of two halves of the segmented lesion obtained from LSM subsystem have been evaluated along both horizontal and vertical axes. The segmented image has been rotated according to the orientation of its principal axis as illustrated in Fig. 11(b). Two halves of the lesion and the folded bottom half have also been shown in Fig. 11(c), (d) and (e) respectively. The difference between the top and folded bottom halves

have been estimated by applying XOR operation on the binary segmented plane as depicted in Fig. 11(f). Inspired by the standard *ABCD* rule elaborated in (Kasmi & Mokrani, 2016) and in consultation with dermatologist involved in this work, deviation of 2% of the estimated number of pixels along any one of the axis has been considered as the shape asymmetry condition is as follows:

$$A_V = \frac{abs|A_L - A_R|}{A} \text{ or } A_H = \frac{abs|A_T - A_B|}{A} > 0.02. \quad (12)$$

Here, A_V corresponds to vertical shape asymmetry determining the deviation of number of pixels between left (A_L) and right half (A_R) with respect to the total area of the lesion (A). Similarly, A_H signifies the horizontal shape asymmetry considering the top (A_T) and bottom half (A_B) of the lesion.

The difference between the average intensity of the two halves (left (L_L) and right (L_R) or top (L_T) and bottom (L_B)) along both horizontal (L_H) and vertical (L_V) axes has been estimated to evaluate the brightness asymmetry of the lesion. In reference to the previous work and the quality of the images considered in this work, the threshold value has been chosen as 3% deviation with respect to the average intensity of the lesion area (L). Therefore, the condition for brightness asymmetry has been given as:

$$L_V = \frac{abs|L_L - L_R|}{L} \text{ or } L_H = \frac{abs|L_T - L_B|}{L} > 0.03. \quad (13)$$

To obtain color asymmetry present in the two halves of the lesion area along horizontal axis and also along vertical axis, each half of the lesion has been subdivided into smaller superpixel regions according to the color information. For the superpixel generation, the SLIC algorithm has been implemented. The number of superpixels has been determined as the ratio of the total number of *ROI* pixels in the corresponding half and the minimum number of pixels to form a superpixel. Here, 32 numbers of pixels have been selected to form a superpixel. The number of superpixels having same median value has been considered as the symmetric color regions. The symmetric and asymmetric color regions in both half of the lesion area along each of the axes have been determined. The lesion has been considered to be color asymmetric along any axis if the number of asymmetric color regions is more than the symmetric color regions along that axis. The entire rule base for the estimation of shape, brightness and color asymmetry has been shown in Fig. 12. The final rule base to determine the asymmetry of the lesion has been shown in Fig. 13.

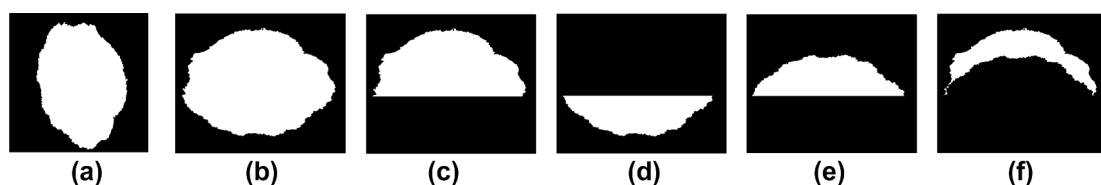
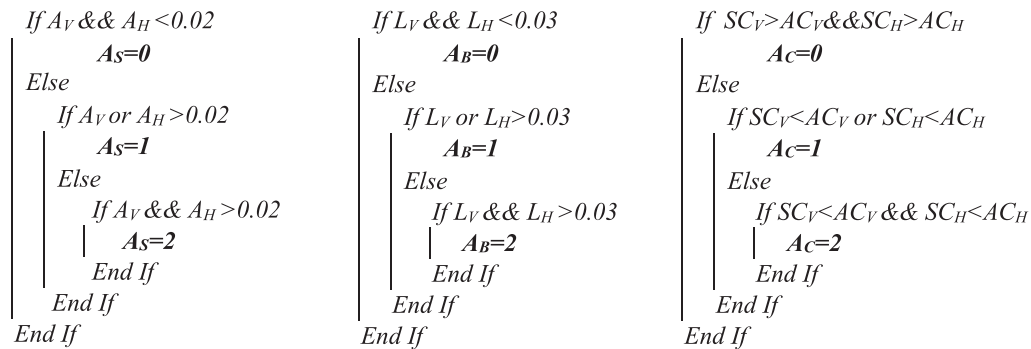


Fig. 11. (a) original segmented image, (b)rotated image, (c) upper half (d) lower half of the segmented image and (e) folded lower half, (f) difference image.



H , V are horizontal and vertical axes respectively. ## As , Ab and Ac are shape, brightness and color asymmetry respectively. ### SC and AC are symmetric and asymmetric colors respectively

Fig. 12. Rule base for estimating shape, brightness and color asymmetry.

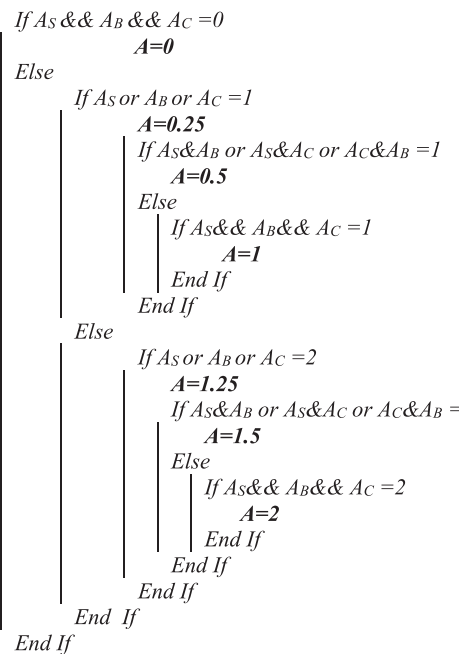


Fig. 13. Rule base for estimating asymmetry of the lesion.

4.1.2. Border irregularity

The border-detected image obtained from BDM subsystem has been subdivided into eight equal segments. In ABCD rule, the border irregularity score between 0 and 8 has been estimated by evaluating the irregularity present in each of the eight segments. If none of the segment has irregularity, then the minimum score of 0 has been considered and a score of 1 has been assigned for the irregularity of each segment up to the maximum score of 8. Here, Katz fractal dimension (Katz, 1988, Chatterjee et al., 2018) has been determined from the border series of each segment. The fractal dimension of a planar curve is:

$$D = \log(P)/\log(d) \quad (14)$$

where, P is the total length of the curve and d is the diameter or planar extent of the curve (Katz, 1988). The total length of the curve is determined as the sum of the distances between successive points of the curve. The diameter d is the maximum distance between the first sample and all the subsequent samples in the time series.

Considering the average step a , i.e. the average distance between the successive points of the time series, number of steps (n) in the time series has been determined as, $n = P/a$.

For n number of steps of the curve of length (P) and diameter (d), the

Katz fractal dimension (Katz, 1988) has been determined as

$$K_D = \frac{\log(n)}{\log(d/P) + \log(n)} \quad (15)$$

The skin lesions are commonly circular in nature. Considering the fractal dimension of a circle as the reference, the irregularity of the lesion has been determined from the deviation of the fractal dimension of that structure with respect to the reference value. The deviation of more than 10% from the reference has been considered to label the segment as irregular.

4.1.3. Color

The CIEM subsystem has provided the information regarding the presence of six different dermatologically significant colors in the lesion area. To calculate the TDS, the score has been assigned as zero for the absence of any of the six colors and maximum score of six for the presence of all of the six colors. For the presence of each distinguished color, a score of one has been assigned.

4.1.4. Differential structures

Here, DSSM sub-system has been developed to extract five dermoscopic structures as pigment network, dots, globules, structureless area and blue-white veil. Minimum score of zero to maximum of five has been assigned for the absence of any structure to the presence of all the five structures, respectively. According to standard ABCD rule, for the presence of each structure, a score of one has been assigned. For pigment network, dots, globules and structureless area, size more than 10% of the entire lesion area has been considered for existence of the structure. The irregular or localized distribution of pigment network, dots and globules in the lesion area is more indicative towards melanoma than globally distributed structures. Considering these dermoscopic findings, here an improvisation on the ABCD rule is proposed, by adding a score of 0.5 for each of the locally distributed structure (pigment network, dots and globules) satisfying the following conditions:

- **Absent Structure:** if the dermoscopic structure (DS) has an area of less than 10% of the total area of the lesion (A_L), then the structure has been considered to be absent (González-Díaz, 2019).

$$\text{Area}(DS) < 0.1 \times A_L \quad (16)$$

- **Local structure:** if the dermoscopic structure contains more than 10% but less than 50% of the total pixels of the lesion area, then the structure has been considered to be locally distributed along the lesion area.

$$0.1 \times A_L < \text{Area}(DS) < 0.5 \times A_L \quad (17)$$

- **Global structure:** if the dermoscopic structure contains more than 50% of the total pixels of the lesion area, then the structure has been considered to be global structure.

$$\text{Area}(DS) > 0.5 \times A_L \quad (18)$$

The presence and absence of the structureless area has been considered by assigning a score of 1 and 0 respectively. The presence of the structureless area is predominant if it occupies more than 10% of the entire lesion area and is considered to be absent otherwise. The spatial information of the structureless area does not have any significant effect on lesion identification. Therefore, no further improvisation is introduced for the estimation of the overall 'D' score considering the spatial properties of the structureless area. Blue-white veil can be found in both malignant and benign lesions. If the blue-white veil area covers a

significant region (more than 30% of the entire lesion area), it is considered as feature for benign lesion. Under such condition, a score of 1 has been added to the entire 'D' score for blue-white veil with more than 10% area of the entire lesion. Similarly, for the structure occupying more than 30% of the entire lesion area, value of 0.5 is subtracted from the entire 'D' score.

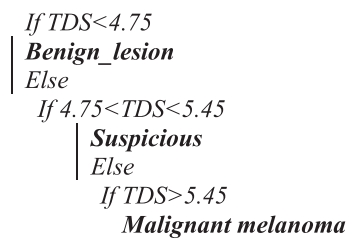
The entire rule base to determine the D score has been shown in Fig. 14.

4.2. Calculation of total dermoscopic score (TDS)

Following the standard ABCD rule of dermatoscopy (Nachbar et al., 1994), TDS is estimated by multiplying the ABCD attributes with the coefficients 1.3, 0.1, 0.5 and 0.5 respectively, as given below.



Fig. 14. Rule base for determining the D score.

**Fig. 15.** Rule based classifier.

$$TDS = A \times 1.3 + B \times 0.1 + C \times 0.5 + D \times 0.5. \quad (19)$$

4.3. Classifier design based on TDS

To classify the diseases based on TDS, the lesions have been categorized into three classes as benign, suspicious and malignant melanoma. The low TDS determines the benign lesions (TDS less than 4.75) while an intermediate score between 4.75 and 5.45 is interpreted as suspicious lesions. A high value of TDS score is considered as a malignant lesion. Here, the threshold values for the differentiation of malignant, benign and suspicious lesions have been selected following the standard ABCD rule of dermoscopy. The rule base for the classifier has been given in Fig. 15.

Using the rule base, the final decision regarding the disease class and associated findings have been obtained by the inference engine.

5. Results and discussion

5.1. Dataset and experimental setup

The expert system for skin disease diagnosis has been evaluated using the official database ISIC challenge 2016, 2017, 2018 dataset (Codella, 2018) and PH2 dataset (Mendonça et al. 2013). The database has 6,669 dermoscopic images, comprising of histopathologically confirmed lesions, malignant melanoma (2,209), nevus (3,430), basal cell carcinoma (BCC) (586), seborrheic keratosis (SK) (419) and squamous cell carcinoma (SCC) (226). The entire dataset is categorized as malignant, benign and suspicious lesions. The dermoscopic images annotated as malignant, including malignant melanoma, malignant BCC (67), SK (1) and SCC (22) are considered for the identification of malignant lesions. The benign category is comprised of nevus (3,422), SK

(418) and benign BCC (1) lesions. Here, some of the identified lesions are not categorized as benign and malignant. Such dermoscopic images considered as suspicious lesions are BCC (518), SCC (204) and nevus (8). Among 6,669 number of dermoscopic images, 2,116 images have been annotated with differential structures (pigment network, dots and globules). Optimum parameter/ threshold values for the estimation of dermoscopic scores, as mentioned in Section 4, have been achieved at after thorough experimentations.

5.2. Comparative performance analysis of the LSM subsystem and State-of-the-art techniques

The performance of the lesion segmentation module (LSM) of the expert system has been compared with the state-of-the-art techniques applied on different datasets having different number of images, and the results are given in table 4 and table 5 respectively.

In this work, all the dermoscopic images have been resized to 512 × 512 pixels and converted to gray scale form. For the development of morphological filters and segmentation algorithm, circular structuring element has been chosen with a size of eight-pixel diameter. Therefore, for the segmentation of the skin lesions, 512 × 512 size of gray scale images with 8-pixel diameter circular structuring elements have been considered as the setting for lesion segmentation module.

The performance of the reported segmentation algorithm has been compared with the state-of-the-art techniques on ISIC challenge 2017 dataset in table 4. It can be observed from table 4 that a deep full resolution convolutional neural network for the segmentation of skin lesions as reported in (Al-Masni et al., 2018) has achieved 0.7711 JSI, 0.8708 DSC and 0.9403 accuracy on 600 test images of ISIC challenge 2017 dataset. In (Bi et al., 2016), 0.9408 accuracy, 0.7773 JSI and 0.8566 DSC have been obtained for the segmentation of the skin lesions employing a deep class-specific learning approach. Performing fully convolutional neural network and dual path network technique for skin lesion segmentation from dermoscopic images by (Shan et al., 2020), it has been reported that the segmentation performance indices are 0.9371 of pixel level accuracy, 0.7634 JSI and 0.8456 DSC. High-resolution convolutional neural network for the segmentation of the skin lesions has been implemented in (Xie et al., 2020) achieving 0.9380 accuracy, 0.7830 JSI and 0.8620 DSC on ISIC 2017 dataset. To compare the reported work with the above mentioned techniques, segmentation performance indices have been evaluated on the same 600 dermoscopic images considered by the other authors. In the work reported in the

Table 4
Comparative Performance Analysis of the LSM subsystem for skin lesion segmentation and state-of-the-art techniques on the ISIC challenge dataset.

Dataset	Method	Segmentation Performance Indices				
		Sen	Spc	ACC	JSI	DSC
ISBI/ISIC 2017 dataset (2000 training images, 600 testing images)	M.A. Al-masni et al., 2018	0.8540	0.9669	0.9403	0.7711	0.8708
	Bi et al., 2018	0.8620	0.9671	0.9408	0.7773	0.8566
	Shan et al., 2020	0.8382	0.9865	0.9371	0.7634	0.8456
	Xie et al., 2020	0.8700	0.9640	0.9380	0.7830	0.8620
	Proposed Method	0.9120	0.9750	0.9480	0.8120	0.8680
ISBI/ISIC2016 dataset (900 training images, 379 testing images)	Bi et al., 2018	0.9311	0.9605	0.9578	0.8592	0.9177
	Xie et al., 2020	0.870	0.964	0.938	0.918	0.858
	Proposed Method	0.946	0.976	0.961	0.874	0.914

Table 5
Comparative Performance Analysis of the LSM subsystem for skin lesion segmentation and state-of-the-art techniques on the PH2 dataset.

Dataset	Method	Segmentation Performance Indices				
		Sen	Spc	ACC	JSI	DSC
PH2 dataset (200 images for testing)	M.A. Al-masni et al., 2018	0.9372	0.9565	0.9508	0.8479	0.9177
	Xie et al., 2020	0.963	0.942	0.949	0.857	0.919
	Shan et al., 2020	0.9477	0.9628	0.9363	0.8351	0.9026
	Bi et al., 2018	0.9623	0.9452	0.9530	0.8590	0.9210
	Proposed Method	0.958	0.982	0.968	0.863	0.912

present paper, the mathematical morphology aided segmentation technique has segregated the lesion area from the dermoscopic images with acceptable performance indices of 0.912 sensitivity, 0.975 specificity, 0.948 accuracy, 0.812 JSI and 0.868 DSC. Table 4 reveals that the reported methodology has outperformed the state-of-the-art segmentation techniques on ISIC challenge 2017 dataset.

The performances of the works by (Bi et al., 2018) and (Xie et al., 2020) have also been tested on ISIC challenge 2016 dataset. The segmentation technique reported by (Bi et al., 2018) has achieved 0.9311 sensitivity, 0.9605 specificity, 0.9578 accuracy, 0.8592 JSI and 0.9177 DSC, evaluated on 379 dermoscopic images. The research work by (Xie et al., 2020) has reported the segmentation performance indices of 0.87 sensitivity, 0.964 specificity, 0.938 accuracy, 0.918 JSI and 0.858 DSC on the ISIC challenge 2016 dataset. To compare the proposed morphology aided segmentation technique with the state-of-the-art techniques, the performance indices have been evaluated on the same set of 379 dermoscopic images of ISIC challenge dataset and it has obtained 0.946 sensitivity, 0.976 specificity, 0.961 accuracy, 0.874 JSI and 0.914 DSC.

The comparative performance analysis of the reported work with some of the published work on PH2 dataset has been tabulated in table 5. The research group led by (M.A. Al-masni et al., 2018) have evaluated the segmentation performance of the reported work on 200 dermoscopic images of PH2 dataset and achieved 0.9372 sensitivity, 0.9565 specificity, 0.9508 accuracy, 0.8479 JSI and 0.9177 DSC. In (Xie et al., 2020), 0.963 sensitivity, 0.942 specificity, 0.949 accuracy, 0.857 JSI and 0.919 DSC have been obtained by using high-resolution convolutional neural network based segmentation technique applied on dermoscopic images of PH2 dataset. On similar dataset, the segmentation technique employing fully convolutional neural network and dual path based approach by (Shan et al., 2020) has achieved 0.9477 sensitivity, 0.9628 specificity, 0.9363 accuracy, 0.8351 JSI and 0.9026 DSC. The work by (Bi et al., 2018) has tested the segmentation performance on 200 dermoscopic images of PH2 dataset with 0.9623 sensitivity, 0.9452 specificity, 0.9530 accuracy, 0.8590 JSI and 0.9210 DSC. To compare the reported segmentation algorithm implemented in LSM subsystem of the DermESy with the state-of-the-art techniques tabulated in table 5, similar set of dermoscopic images have been considered. Tested on the 200 dermoscopic images of PH2 dataset, the reported segmentation algorithm has achieved 0.958 sensitivity, 0.982 specificity, 0.968 accuracy, 0.863 JSI and 0.912 DSC. Table 5 demonstrates that the report work significantly improves the segmentation performance of the other reported segmentation algorithms, tested on PH2 dataset.

Therefore, the advantage of this morphological segmentation technique is to segment various skin lesions with higher performance indices with lesser computational complexity. The performance metrics of the system for the segmentation of wide varieties of skin lesions, complex structures endorse the robustness of the system.

True Class	Predicted Class		
	M	S	B
M	2246	15	38
S	243	175	312
B	36	42	3763

(a)

True Class	Predicted Class		
	M	S	B
M	1973	227	99
S	79	613	38
B	84	148	3609

(b)

Fig. 16. (a) Confusion matrix of DermESy, (b)confusion matrix of Expert's diagnosis.

$$SE = \frac{\text{No. of True Positive (TP) skin disease samples}}{\text{No. of all skin disease samples classified as positive (TP + FN)}} \quad (20)$$

$$SP = \frac{\text{No. of True Negative (TN) skin disease samples}}{\text{No. of all skin disease samples classified as negative (TN + FP)}} \quad (21)$$

$$ACC = \frac{\text{No. of correctly classified skin disease samples (TP + TN)}}{\text{Total No. of skin disease samples (TP + TN + FP + FN)}} \quad (22)$$

where, TP = Positive samples classified as positive; TN = Negative samples classified as negative; FP = Negative samples misclassified as positive; FN = Positive samples misclassified as negative (Chatterjee et al., 2019).

The comparative analysis of the dermatologist's performance with the expert system has been depicted in Fig. 17. The expert system has differentiated the malignant and benign lesions with 97.69% sensitivity, 97.97% specificity and 97.86% accuracy. Dermatologist has detected the malignant and benign lesions with 85.82% of sensitivity, 93.96% specificity and 90.91% accuracy. From Fig. 17, it has been observed that the quantification of the dermoscopic findings has improved the skin disease identification performance significantly. The proper estimation of the TDS has reduced the number of suspicious lesions leading to the enhanced identification accuracy for deciding the further course of treatment.

The methodology illustrated in (Piccolo et al., 2014), have tested the diagnosis of malignant melanoma from 165 pigmented skin lesions with a Kappa value, a score measuring the agreement between two or more human evaluators of 0.96 employing ABCD rule. The results have been verified with three experts having different spans of experience. However, the performance of the system has been evaluated on a very small dataset, with minimum variability in samples in comparison with this present work. An ABCD rule based system has been developed by (Smaoui & Bessassi, 2013) estimating morphological features, colors and diameter of the lesions. The work has reported 92% classification accuracy for 40 dermoscopic images. The present research work has improvised the attributes of the ABCD rule and considering the differential structures 97.87% accuracy has been achieved for 6669 dermoscopic images. As reported in (Kasmi & Mokrani, 2016), 94% accuracy has been achieved for the differentiation of malignant and benign skin lesions on the basis of ABCD rule. In that proposed methodology, the dermoscopic structures have not been segmented for proper visual inspection by the dermatologists. For the estimation of ABCD attributes, the spatial information of the dermoscopic structures have not been considered. However, in this present work, the TDS has been estimated with improvised ABCD attributes considering the spatial information of the dermoscopic structures. The performance of this reported work has also been verified with the diagnostic performance indices with an expert dermatologist. The skin disease diagnosis technique described in

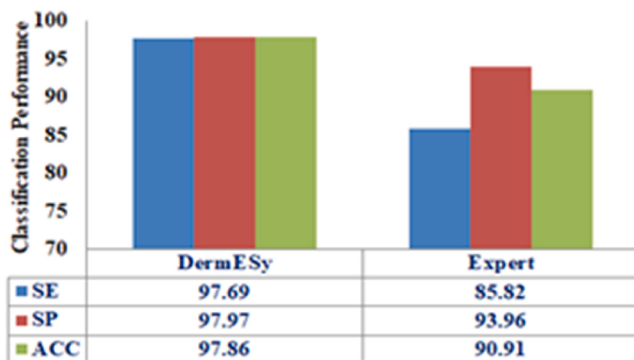


Fig. 17. Performance comparison between DermESy and Expert's Diagnosis.

(González-Díaz, 2019) has developed a knowledge based CNN model for skin disease diagnosis. This technique has not incorporated a proper segmentation method for extraction of features related to the structural properties of the lesions. An appropriate visualization module for the identification of dermoscopic findings has not been introduced in the model. However, DermESy is developed considering a segmentation module for accurate segmentation of skin lesion area to estimate asymmetry index of the lesion and also to monitor further spreading of the disease. In this model, an explanatory subsystem is introduced to recognize the dermoscopic finding related to the ABCD rule of dermoscopy and to correlate the decision with an expert dermatologist. A graphical user interface of the developed expert system is shown in Fig. 18. Doctor can use this system to visualize the segmented lesion area, its border, color regions and other differential structures for further assessment and monitoring of the disease. Computer aided classification system has been developed to differentiate suspicious and non-suspicious pigmented lesions using ABCD features by (Birkenfeld et al., 2020). The authors have considered 1759 wide-field images, acquired by a consumer grade camera instead of dermoscopic images. According to the dermatologist associated with the present research group, naked eye examination of the lesion shows more invasiveness of a malignant lesion compared to a benign one as the cells are rapidly dividing. Magnified images were taken into consideration to raise the suspicion of malignancy in a better way. 'D' of ABCD rule stands for diameter or differential structure obtained from dermoscopic images only. For clinical images, consideration of diameter is enough to suspect the malignancy of the lesion followed by a biopsy for confirmation. Dermoscopic images provide in-depth visualization of color and differential structures of the lesions. Considering this, dermoscopic images have been used here to extract color and differential structures from the lesion area to evaluate 'C' and 'D' attributes of ABCD rule. The authors (Birkenfeld et al., 2020) have extracted different texture features using state-of-the-art techniques. However, literature suggests that the information regarding the presence of differential structures in skin lesions cannot be assessed through existing texture analysis tools. In the work presented here, various image processing tools have been employed to extract the differential structures present in the lesion and accordingly the ABCD rule has been improvised by considering not only the existence of the structures but also their spatial properties. The reported DermESy has differentiated malignant and benign lesions with 97.86% accuracy compared to the accuracy of 75.9% reported in (Birkenfeld et al., 2020). The work by (Gola Isasi et al., 2011) focuses primarily on the development of different pattern recognition algorithms to extract globular, reticular and blue-veil patterns from the skin lesions. Apart from extracting such differential structures, an indigenous expert system has also been developed in the present work for proper estimation of the ABCD scores with a rule based classifier to provide a second opinion for improved diagnosis and monitoring of the disease. The reported algorithms (Gola Isasi et al., 2011) have been employed in 160 dermoscopic images whereas the present expert system considers 6669 dermoscopic images for the extensive analysis of all ABCD attributes and the diagnosis of the diseases. An ABCD rule based pigmented skin lesion identification technique has been developed by (Mabrouk et al., 2020). The authors have used ABCD feature based SVM classification technique for the differentiation of malignant and benign lesions from 320 dermoscopic images. In this reported DermESy system, total dermoscopic score has been evaluated with improvised ABCD attributes for the development of rule based classifier as compared to the technique introduced by (Mabrouk et al., 2020). For the estimation of ABCD attributes, significant improvisation has been introduced by incorporating the consideration of shape, brightness and color asymmetry of the lesion along with spatial properties of dermoscopic structures. In this present work, to bring out considerable color information from the skin lesion area, a superpixel based color information extraction module is introduced by considering the colors of the corresponding expert's annotated regions as reference. In comparison to the work (Mabrouk et al., 2020), in the

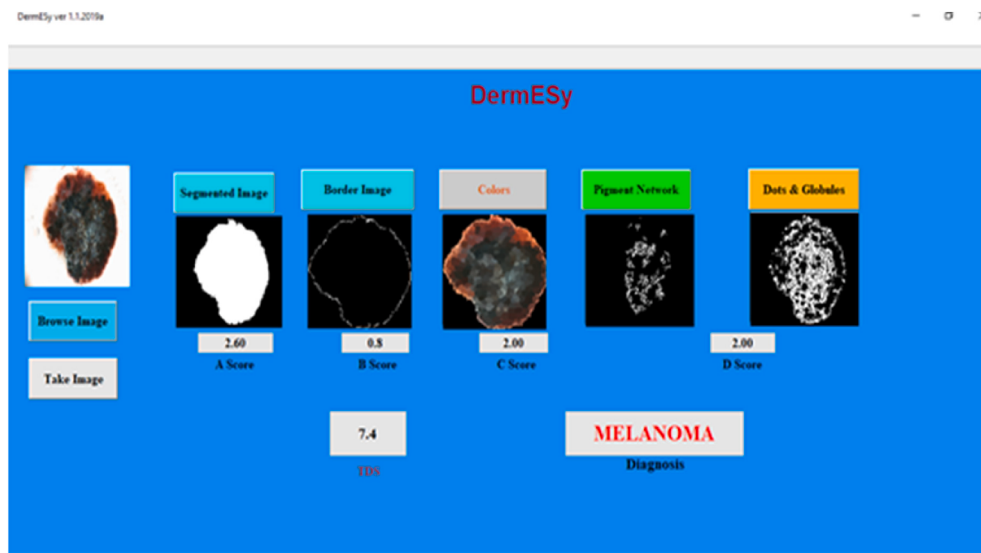


Fig. 18. Graphical user interface (GUI) of the DermESy, an expert system implementing ABCD rule of dermoscopy.

present study five differential structures have been identified as pigment network, dots, globules, structureless area and blue-white veil, for the evaluation of 'D' score of ABCD rule of dermoscopy. The performance of the DermESy has been evaluated on 6669 dermoscopic images of various disease classes that justifies the robustness of the system.

The reported dermatological expert system has been envisaged as a fully automated system irrespective of the datasets involved. It has been developed by considering the dermoscopic images of ISIC archive database and PH2 Dataset (as described in Section 5.1). Therefore, a large number of samples with wide varieties of diseases have been incorporated for the identification of malignant and benign lesions. Dermatological expert system has automatically differentiated malignant, benign and suspicious categories of the sample dermoscopic images irrespective of the image source following the same steps and parameter settings. Acceptable performance indices for all the images from various resources with different image acquisition techniques affirmed the robustness of the system. Hence, it may be expected that the

method can work with reasonable performance metrics irrespective of the datasets involved.

5.4. Comparative analysis of dermoscopic findings of DermESy with Expert's opinion

Employing the DermESy technique, ABCD attributes of the ABCD rule of dermoscopy have been estimated by finding different colors, structures and quantification of morphological properties of the lesion. Presence of white (W), red (R), light brown (LB), dark brown (DB), blue-gray (BG) and Black (B) colors helps to identify the malignant lesions at an early stage of the disease. Also, the structural asymmetry of the lesion is a very important parameter to identify the character of the lesion. Presence of different differential structures, predominantly the pigment network and the dots and globules identify the malignant lesions. In Fig. 19, a set of sample dermoscopic images have been shown along with their corresponding dermoscopic findings obtained using DermESy and

Sample Image	DermESy/ Expert	A				B				C				D			
		Asy	B	W	R	LB	DB	BG	B	PN	Dots	Globules	BWV	SL			
	DermESy	P	P	P	A	P	P	P	P	P	A	A	P	P	P	P	
	Expert	P	P	P	A	P	P	P	P	P	P	A	P	P	P	P	
	DermESy	P	P	A	A	P	P	A	P	P	P	A	A	A	A	A	
	Expert	P	P	A	A	P	P	A	A	P	P	A	A	A	A	A	
	DermESy	P	P	P	A	P	P	P	P	P	P	P	A	A	A	A	
	Expert	P	P	P	A	P	P	P	P	P	P	P	P	P	P	P	
	DermESy	A	A	A	A	P	P	A	A	P	P	A	A	A	A	A	
	Expert	P	P	A	A	P	A	A	A	A	P	A	A	A	A	A	
	DermESy	A	A	A	A	P	P	A	P	P	A	A	A	A	A	A	
	Expert	A	A	A	A	P	P	A	P	P	P	P	A	A	P	A	

Fig. 19. Identification of ABCD attributes from sample dermoscopic images using DermESy (BWV- Blue-white veil; SL- Structureless area; P- Present; A- Absent).

expert dermatologist. The figure depicts the presence of all the six colors in the lesion area and illustrates the multiplicity of colors in malignant lesions compared to the benign lesions. The findings of color information have been verified with dermatologist's findings as shown in the figure. It justifies the correlation between the dermatologist opinion and findings of DermESy. It illustrates the presence of five differential structures obtained by DermESy. From the figure, it has been observed that structures extracted by the DermESy from most of the dermoscopic images have been confirmed by the expert. It also describes that the presence of pigment network and its spatial distribution has differentiated the malignant and benign lesions. Considering the spatial distribution of differential structures along the lesion, the ABCD rule has been improvised to evaluate total dermoscopic score for the identification of the lesion. Morphological properties of skin lesions have been evaluated using DermESy as shown in Fig. 19. It depicts the lower asymmetry index and structural irregularity present in the lesion that leads to the identification of benign skin diseases. From the figure, it has been perceived that DermESy has identified some of the color and structural properties, which have not been detected from visual inspection by the dermatologist. Using DermESy, identification of various important dermoscopic findings and proper estimation of morphological properties of the lesion helps to determine the total dermoscopic score more precisely for early stage diagnosis of the diseases. Much better identification of ABCD attributes helps the dermatologist to correlate the dermoscopic findings and further analysis of the disease.

5.5. Performance comparison of DermESy with state-of-the-art automatic systems

In the present work, the dermoscopic images have been collected from ISIC challenge (2016, 2017, 2018) and PH2 dataset. Among 6669 dermoscopic images, 200 images are from PH2 dataset (160 benign and 40 malignant lesions) and remaining 6469 images are from ISIC challenge dataset. ISIC dataset comprises of dermoscopic images for 2016, 2017 and 2018 challenge. ISIC 2016 challenge dataset contains 1279 dermoscopic images (900 training images and 379 testing images). In ISIC 2017 challenge dataset, additional 1696 dermoscopic images have been included. Remaining 3494 dermoscopic images collected for this work are from ISIC 2018 challenge dataset. For the characterization of the skin lesions using DermESy, ABCD attributes have been determined from each of the dermoscopic images to estimate the corresponding TDS. Depending on the TDS parameter value, the dermoscopic images have been classified as malignant, benign and suspicious category. For TDS value less than 4.75, the lesions are classified as benign and for value more than 5.45, the lesions are classified as malignant. The TDS value within 4.75 and 5.45 corresponds to suspicious lesion category. Considering these parameter settings of the TDS score, the dermoscopic images of ISIC and PH2 datasets have been classified separately to compare the performance of DermESy with state-of-the-art techniques applied on the same datasets.

An integrated deep convolutional network based approach has been introduced by (Al-masni et al., 2020) to classify skin lesions from ISIC challenge 2016 dataset. The reported deep convolutional network based

technique has obtained 81.79% classification accuracy for 379 test images. To compare the classification performance of the DermESy with the work by (Al-masni et al., 2020), the same set of dermoscopic images has been considered. Evaluating the TDS score from corresponding ABCD attributes from each of the 379 dermoscopic images, the skin lesions have been classified with 98.62% accuracy. The same work of (Al-masni et al., 2020) has tested the classification performance on ISIC 2017 dataset and obtained 81.57% accuracy. An ensemble deep convolutional neural networks has been used by (Harangi, 2018) to classify the skin abnormalities from the available dermoscopic images of ISIC challenge 2017 dataset. The authors (Harangi, 2018) have evaluated the performance on 600 testing images and obtained 86.60% classification accuracy. The work by (Mahbod et al., 2019) has proposed a combination of intra-architecture and inter-architecture network fusion using convolutional neural network for the identification of skin diseases on the same ISIC 2017 dataset. The authors have reported 87.70% classification accuracy by considering same set of images for testing purpose. The performance of the reported work has been compared with these state-of-the-art techniques, applied on same ISIC challenge 2017 dataset and has achieved 97.84% accuracy. A generative adversarial network (GAN) based system has been employed by (Qin et al., 2020) to classify the skin lesions from ISIC 2018 dataset. The work has achieved 95.20% classification accuracy by considering 2003 number of test images of ISIC 2018 dataset. The work by (Al-masni et al., 2020) has also evaluated the classification performance on the same 2003 2003 dermoscopic images of ISIC challenge 2018 dataset and has reported 89.28% accuracy. The reported work has also been tested on the same 2003 number of dermoscopic images and has obtained the classification accuracy of 97.02%. Table 6 reveals that the reported expert system has outperformed the state-of-the-art methodologies for the identification of skin diseases with higher degree of accuracy on ISIC challenge 2016, 2017 and 2018 datasets.

In table 7, the performance of the reported dermatological expert system has been compared with some of the recently published works for skin disease classification on publicly available PH2 dataset. A diagnostic system for melanoma identification using ABCD rule of dermoscopy has been reported by (Zaqout, 2019). The author (Zaqout, 2019) has reported 90% accuracy for melanoma identification from 200 dermoscopic images of PH2 dataset, which has not been verified with an expert's opinion, in contrast to this present approach. A stacking ensemble method based on the Meta Learning algorithm has been proposed by (Ghalejoogh et al., 2020) for the classification of skin abnormalities. The reported work (Ghalejoogh et al., 2020) has classified the skin lesions from the dermoscopic images of PH2 dataset with 96% classification accuracy. The research work by (Hu et al., 2019) has introduced bag-of-feature model using feature similarity measurement technique based on codebook learning algorithm for the classification of melanoma from the dermoscopic images of PH2 dataset. In this work (Hu et al., 2019), 91.90% accuracy has been attained for the classification of skin lesions. A support vector machine classifier based skin disease identification technique has been proposed by (Gulati & Bhogal, 2020) and obtained 94.50% classification accuracy. To compare the classification performance of the reported expert system with state-of-

Table 6
Classification performance comparison of the proposed system with state-of-the-art techniques on ISIC challenge dataset.

Dataset	Method	Classification Accuracy (%)
ISBI/ISIC 2016 Dataset(900 training images, 379 testing images)	M.A. Al-masni et al., 2020	81.79
	Proposed Method	98.62
ISBI/ ISIC 2017 dataset (2000 training images, 600 testing images)	M.A. Al-masni et al., 2020	81.57
	Harangi, 2018	86.60
	Mahbod et al., 2019	87.70
	Proposed Method	97.84
ISBI/ ISIC2018 dataset (Total 10,015 no of images, 2003 images for testing)	Qin et. al, 2020	95.20
	M.A. Al-masni et al., 2020	89.28
	Proposed Method	97.02

Table 7

Classification performance comparison of the proposed system with state-of-the-art techniques on PH2 dataset.

Dataset	Method	Classification Accuracy (%)
PH2 Dataset (200 images for testing)	Zaqout, 2019	90.00
	Ghalejoogh et al., 2020	96.00
	Hu et al., 2019	91.90
	Gulati & Bhogal, 2020	94.50
	Proposed Method	98.48

Sample Images	Diagnosis by DermESy		Diagnosis by Dermatologist	
	TDS	Category	TDS	Category
	6.50	Malignant	6.00	Malignant
	5.85	Malignant	5.05	Suspicious
	5.60	Malignant	4.90	Suspicious
	4.25	Benign	5.00	Suspicious
	6.25	Malignant	5.85	Malignant
	4.00	Benign	4.25	Benign

Fig. 20. Comparative analysis of the diagnosis of skin lesions using DermESy and Expert Dermatologist.

the-art techniques on PH2 dataset, TDS value has been estimated from each of the 200 dermoscopic images. Based on the TDS value, the skin lesions have been identified with 98.48% accuracy. Table 7 portrays that the reported ABCD rule based expert system has achieved an acceptable classification accuracy for skin disease diagnosis from PH2 dataset. The results have described a significant improvement in classification performance compared to the recently published works on same dataset.

5.6. Comparative analysis of the diagnosis of skin lesions using DermESy and expert dermatologist

A graphical user interface of the developed expert system is shown in Fig. 18. Doctor can use this system to visualize the segmented lesion area, its border, color regions and other differential structures for further assessment and monitoring of the disease.

The performance of the expert system is compared with the expert's diagnosis for establishing the robustness of the algorithms. Dermatologist of this research group has identified the malignant and benign lesions from the dermoscopic image set. Dermatologist has determined the corresponding TDS of each lesion based on their clinical criteria described by ABCD attributes. Fig. 20 has depicted the diagnosis of skin lesions using DermESy and the dermatologist involved in this work. The

corresponding TDS score evaluated by the dermatologist and DermESy have been given for the ready reference. From the figure, it has been observed that improvisation of ABCD attributes in DermESy helps to categorize suspicious lesion into malignant or benign class. Similarly, identification of a set of lesions using DermESy is in line with the diagnosis of the dermatologist. Therefore, the diagnosis of the skin lesion by DermESy can be used as a second opinion apart from the expert's opinion for further decision making.

6. Conclusion

The paper introduces an expert system for skin disease diagnosis. The dermatological expert system has implemented the standard ABCD rule of dermoscopy with significant improvisations. For the estimation of lesion asymmetry score, shape, color and brightness asymmetry have been evaluated. To incorporate dermatologist's expertise, the color information extraction algorithm has been introduced by considering the expert's annotated color information as reference. Dermatologists consider the spatial information of the differential structures to differentiate the malignant and benign lesions. This expertise has been introduced to improvise the ABCD criteria by considering spatial information of the structures to determine the 'D' score. The rule base of

the system has been developed by incorporating the expert dermatologists' knowledge for improved early-stage diagnosis of the disease and further decision making. The incorporation and implementation of ABCD rule of the skin disease diagnosis has provided an in-depth visualization and quantification of dermoscopic findings for further course of action. The performance of the DermESy has been compared with the expert dermatologist's diagnosis on a large set of dermoscopic images. DermESy has identified the malignant and benign lesions with 97.86% sensitivity in comparison with the dermatologist's diagnostic accuracy of 90.91%. Since the performance of the proposed system is evaluated on a large set of images and the diagnosis is also compared with that by a dermatologist, the robustness of the system is ensured. Therefore, DermESy could be an effective tool not only for an expert dermatologist but also for the radiologist or a general physician to evaluate competently the state of the lesion area for further treatment. In future, this DermESy system can be improved for the development of more sophisticated software to provide second opinion to the dermatologists for improved and uniform diagnosis of the disease at an early stage. This work can be extended with required modifications and inclusion of diameter estimation of the lesion for the differentiation of malignant and benign lesions from clinical or macroscopic images. Advanced digital signal processing tools can be introduced to implement this work for remote monitoring of the skin diseases. A microcontroller based integrated system can also be developed implementing the reported DermESy system for the construction of a hand-held device for skin disease monitoring.

CRediT authorship contribution statement

Saptarshi Chatterjee: Conceptualization, Methodology, Software, Formal analysis, Investigation, Writing - original draft. **Debangshu Dey:** Data curation, Resources, Supervision, Project administration, Writing - review & editing. **Sugata Munshi:** Resources, Supervision, Writing - review & editing. **Surajit Gorai:** Data curation, Formal analysis, Validation.

Declaration of Competing Interest

The authors declare that they have no known competing financial interests or personal relationships that could have appeared to influence the work reported in this paper.

Acknowledgement

This work is supported by the Ministry of Electronics and IT, Govt. of India through 'Visvesvaraya PhD scheme' awarded to Jadavpur University, India. The authors would also like to acknowledgement ISIC: ISIC archive dataset for kindly allowing the authors to access the image database for this work.

References

- Achanta, R., Shaji, A., Smith, K., Lucchi, A., Fua, P., & Süsstrunk, S. (2010). SLIC Superpixels. *EPFL Technical Report*, 149300.
- Al-masni, M. A., Al-antari, M. A., Choi, M.-T., Han, S.-M., & Kim, T.-S. (2018). Skin lesion segmentation in dermoscopy images via deep full resolution convolutional networks. *Computer Methods and Programs in Biomedicine*, 162, 221–231.
- Al-masni, M. A., Kim, D.-H., & Kim, T.-S. (2020). Multiple skin lesions diagnostics via integrated deep convolutional networks for segmentation and classification. *Computer Methods and Programs in Biomedicine*, 190, 105351. <https://doi.org/10.1016/j.cmpb.2020.105351>
- Argenziano, G., Fabbrocini, G., Carli, P., De Giorgi, V., Sammarco, E., & Delfino, M. (1998). Epiluminescence Microscopy for the Diagnosis of Doubtful Melanocytic Skin Lesions: Comparison of the ABCD Rule of Dermatoscopy and a New 7-Point Checklist Based on Pattern Analysis. *Arch Dermatol*, 134(12). <https://doi.org/10.1001/archderm.134.12.1563>
- Barata, C., Marques, J. S., & Rozeira, J. (2012). A System for the Detection of Pigment Network in Dermoscopy Images Using Directional Filters. *IEEE Trans. Biomed. Eng.*, 59(10), 2744–2754.
- Bi, J. Kim, E. Ahn Kumar & Fulham, M., Step-wise integration of deep class-specific learning for dermoscopic image segmentation. *Pattern Recognition* 85 2018 78 89.
- Bi, L., Kim, J., Ahn, E., Feng, D., & Fulham, M. (2016). Automated skin lesion segmentation via image-wise supervised learning and multi-scale superpixel based cellular automata, in. In *IEEE 13th International Symposium on Biomedical Imaging (ISBI)* (pp. 1059–1062).
- Birkenfeld, J. S., Tucker-Schwartz, J. M., Soenksen, L. R., Avilés-Izquierdo, José. A., & Martí-Fuster, B. (2020). Computer-aided classification of suspicious pigmented lesions using wide-field images. *Computer Methods and Programs in Biomedicine*, 195, 105631. <https://doi.org/10.1016/j.cmpb.2020.105631>
- Chandaka, S., Chatterjee, A., & Munshi, S. (2009). Cross-correlation aided support vector machine classifier for classification of EEG signals. *Expert Systems with Applications*, 36(2), 1329–1336.
- Chatterjee, S., Dey, D., & Munshi, S. (2018). Optimal selection of features using wavelet fractal descriptors and automatic correlation bias reduction for classifying skin lesions. *Biomedical Signal Processing and Control*, 40, 252–262.
- Chatterjee, S., Dey, D., & Munshi, S. (2019a). Integration of morphological preprocessing and fractal based feature extraction with recursive feature elimination for skin lesion types classification. *Computer Methods and Programs in Biomedicine*, 178, 201–218.
- Chatterjee, S., Dey, D., Munshi, S., & Gorai, S. (2019b). Extraction of features from cross correlation in space and frequency domains for classification of skin lesions. *Biomedical Signal Processing and Control*, 53, 101581. <https://doi.org/10.1016/j.bspc.2019.101581>
- [dataset] Codella, N. C. F., Gutman, D., Celebi, M. E., Helba, B., Marchetti, M.A., Dusza, S.W., Kalloo, A., Liopyris, K. ; Mishra, N. , Kittler, H. & Halpern, A. (2018). Skin lesion analysis toward melanoma detection: A challenge at the 2017 International symposium on biomedical imaging (ISBI), hosted by the international skin imaging collaboration (ISIC). 2018 IEEE 15th International Symposium on Biomedical Imaging (ISBI) 2018, April, 4-7, 2018. Washington, DC, 168–172.
- Ghalejooh, G. S., Kordy, H. M., & Ebrahimi, F. (2020). A hierarchical structure based on Stacking approach for skin lesion classification. *Expert Systems with Applications*, 145, 113127. <https://doi.org/10.1016/j.eswa.2019.113127>
- González-Díaz, I. (2019). DermaKNet: Incorporating the Knowledge of Dermatologists to Convolutional Neural Networks for Skin Disease Diagnosis. *IEEE J. Biomed. Health Inform.*, 23, 547–559.
- Gu, Z., Cheng, J., Fu, H., Zhou, K., Hao, H., Zhao, Y., Zhang, T., Gao, S., & Liu, J. (2019). CE-Net: Context Encoder Network for 2D Medical Image Segmentation. *IEEE Trans. Med. Imaging*, 38(10), 2281–2292.
- Gulati, S., & Bhogal, R. K. (2020). Classification of Melanoma from Dermoscopic Images Using Machine Learning. *Smart Innovation, Systems and Technologies*, 159, 345–354.
- Harangi, B. (2018). Skin lesion classification with ensembles of deep convolutional neural networks. *Journal of Biomedical Informatics*, 86, 25–32.
- Hu, K., Niu, X., Liu, S., Zhang, Y., Cao, C., Xiao, F., Yang, W., & Gao, X. (2019). Classification of melanoma based on feature similarity measurement for codebook learning in the bag-of-features model. *Biomedical Signal Processing and Control*, 51, 200–209.
- Gola Isasi, A., García Zapirain, B., & Méndez Zorrilla, A. (2011). Melanomas non-invasive diagnosis application based on the ABCD rule and pattern recognition image processing algorithms. *Computers in Biology and Medicine*, 41(9), 742–755.
- Kasmi R. & Mokrani, K. (2016). Classification of malignant melanoma and benign skin lesions: implementation of automatic ABCD rule. *IET Image Process.*, 10, 448–455.
- Katz, M. J. (1988). Fractals and the analysis of waveforms. *Computers in Biology and Medicine*, 18(3), 145–156.
- Kawahara, J., & Hamarneh, G. (2019). Fully Convolutional Neural Networks to Detect Clinical Dermoscopic Features. *IEEE J. Biomed. Health Inform.*, 23(2), 578–585.
- Kawahara, J., Daneshvar, S., Argenziano, G., & Hamarneh, G. (2019). 7-point Checklist and Skin Lesion Classification using Multi-Task Multi-Modal Neural Nets. *IEEE J. Biomed. Health Inform.*, 23, 538–546.
- Ma, Z., & Tavares, João. M. R. S. (2017). Effective features to classify skin lesions in dermoscopic images. *Expert Systems with Applications*, 84, 92–101.
- Mabrouk, M. S., Sayed, A. Y., Afifi, H. M., Sheha, M. A., & Sharwy, A. (2020). Fully Automated Approach for Early Detection of Pigmented Skin Lesion Diagnosis Using ABCD. *J. Health Inform Res*, 4(2), 151–173.
- Mahbod, A., Schaefer, G., Ellinger, I., Ecker, R., Pitiot, A., & Wang, C. (2019). Fusing fine-tuned deep features for skin lesion classification. *Computerized Medical Imaging and Graphics*, 71, 19–29.
- Marks, R. (1995). An overview of skin cancers: Incidence and causation. *Cancer Suppl*, 75, 607–612.
- [dataset] Mendonça, T., Ferreira, P. M., Marques, J., Marcal, A. R. S. & Rozeira, J. (2013). PH2 - A dermoscopic image database for research and benchmarking. 35th International Conference of the IEEE Engineering in Medicine and Biology Society, July 3-7, 2013, Osaka, Japan.
- Nachbar, F., Stolz, W., Merkle, T., Cognetta, A. B., Vogt, T., Landthaler, M., Bilek, P., Braun-Falco, O., & Plewig, G. (1994). The ABCD rule of dermatoscopy. *Journal of the American Academy of Dermatology*, 30(4), 551–559.
- Oliveira, R. B., Marranghello, N., Pereira, A. S., & Tavares, João. M. R. S. (2016). A computational approach for detecting pigmented skin lesions in macroscopic images. *Expert Systems with Applications*, 61, 53–63.
- Pal, S., Chatterjee, S., Dey, D., & Munshi, S. (2019). Morphological operations with iterative rotation of structuring elements for segmentation of retinal vessel structures. *Multidim Syst Sign Process*, 30(1), 373–389.
- Pathan, S., Prabhu, K. G., & Siddalingaswamy, P. C. (2018). A methodological approach to classify typical and atypical pigment network patterns for melanoma diagnosis. *Biomedical Signal Processing and Control*, 44, 25–37.

- Pehamberger, H., Binder, M., Steiner, A., & Wolff, K. (1993). In vivo epiluminescence microscopy: Improvement of early diagnosis of melanoma. *J. Invest. Dermatol.*, *100*, 356S–362S.
- Piccolo, D., Crisman, G., Schoinas, S., Altamura, D., & Peris, K. (2014). Computer-automated ABCD versus dermatologists with different degrees of experience in dermoscopy. *Eur. J. Dermatol.*, *24*, 477–481.
- Qin, Z., Liu, Z., Zhu, P., & Xue, Y. (2020). A GAN-based image synthesis method for skin lesion classification. *Computer Methods and Programs in Biomedicine*, *195*, 105568. <https://doi.org/10.1016/j.cmpb.2020.105568>
- Shan, P., Wang, Y., Fu, C., Song, W., & Chen, J. (2020). Automatic skin lesion segmentation based on FC-DPN. *Computers in Biology and Medicine*, *123*, 103762. <https://doi.org/10.1016/j.combiomed.2020.103762>
- Smaoui, N., & Bessassi, S. (2013). A developed system for melanoma diagnosis. *Int. J. Comput. Vis. Signal Process.*, *3*, 10–17.
- Soille, P. (Ed.). (2004). *Morphological Image Analysis*. Berlin, Heidelberg: Springer Berlin Heidelberg.
- Wahba, M. A., Ashour, A. S., Guo, Y., Napoleon, S. A., & Elnaby, M. M. A. (2018). A novel cumulative level difference mean based GLDM and modified ABCD features ranked using eigenvector centrality approach for four skin lesion types classification. *Computer Methods and Programs in Biomedicine*, *165*, 163–174.
- Xie, F., Yang, J., Liu, J., Jiang, Z., Zheng, Y., & Wang, Y. (2020). Skin lesion segmentation using high-resolution convolutional neural network. *Computer Methods and Programs in Biomedicine*, *186*, 105241. <https://doi.org/10.1016/j.cmpb.2019.105241>
- Yuan, Y., & Lo, Y.-C. (2019). Improving Dermoscopic Image Segmentation With Enhanced Convolutional-Deconvolutional Networks. *IEEE J. Biomed. Health Inform.*, *23*(2), 519–526.
- Zaqout, I. (2019). Diagnosis of Skin Lesions Based on Dermoscopic Images Using Image Processing Techniques. *InTechOpen*. <https://doi.org/10.5772/intechopen.88065>